

Electromagnetic Field Produced in High Energy Small Collision System within Charge Density Models of Nucleon

Zong-Wei Zhang,¹ Xian-Zhuo Cen,^{1,2} and Wei-Tian Deng^{1,*}

¹*School of Physics, Huazhong University of Science and Technology, Wuhan 430074, China*

²*Dalingshan Secondary School, DongGuan 523000, China*

Recent experiments show that $\Delta\gamma$, an observable designed for detecting the chiral magnetic effect (CME), in small collision system $p + A$ is similar with that in heavy ion collision $A + A$. This brings a challenge to the existence of CME because it is believed that there is no azimuthal correlation between the orientation of the magnetic field (Φ_B) and the participant plane (Φ_2) in small collision system. In this work, we introduce three charge density models to describe the inner charge distributions of proton and neutron, and calculate the electric and magnetic fields produced in small $p + A$ collisions at both RHIC and LHC energies. Our results show that the contribution of the single projectile proton to the magnetic field is the main source after average over all participants. The azimuthal correlation between Φ_B and Φ_2 is small but not vanished. And due to the huge fluctuation of fields strength, the magnetic-field contribution to $\Delta\gamma$ could be large.

I. INTRODUCTION

In high energy heavy ion collisions, quark-gluon-plasma (QGP) is produced due to the extreme environment of high temperature and high pressure. Since the colliding large ions have positive electric charge, a strong transient electric and magnetic fields are also produced [1–8] in off-central collisions. This extremely strong fields provide a unique environment to study properties of quantum chromodynamics (QCD). People have realized that there maybe is a parity symmetry(\mathcal{P}) or charge conjugate and parity symmetry(\mathcal{CP}) violation effect in QCD [9–14]. This effect could be observed as chiral magnetic effect (CME) once coupled to a strong magnetic field [11, 12]. The high energy heavy-ion collision could give an excellent environment for studying CME, because not only the QGP with high temperature could be generated but also an extremely strong magnetic field is produced. Search of CME is one of the most important tasks of high energy heavy ion collision physics. The measurement of the charge separation phenomenon induced by CME can provide a way to study the quantum anomaly of QCD vacuum topology.

However, the charge separation phenomenon cannot be directly observed, so a three-point correlator

$$\gamma = \langle \cos(\alpha + \beta - 2\Phi_2) \rangle \quad (1.1)$$

was proposed [15], where α and β is azimuthal angles of charged particle, the Φ_2 is the angle of the reaction plane for a given case. Significant charge distribution anisotropy $\Delta\gamma$

$$\Delta\gamma \equiv \gamma_{OS} - \gamma_{SS} \quad (1.2)$$

has indeed been measured in heavy-ion collision experiments [16–20] which show features consistent with the CME expectation. Here, γ_{OS} represents for opposite charge particle pair, γ_{SS} represents for same

* dengwt@hust.edu.cn

charge particle pair. However, this observable may include the effect induced by elliptic-flow (v_2) induced backgrounds [21–26]. The CME and v_2 -related background are driven by different physical mechanisms: the CME is very closely related to magnetic field, but v_2 -related background is connected to the participant plane: Φ_2 .

The charge anisotropy is related not only the strength of fields, but also the azimuthal correlation between Φ_B and Φ_2 [27, 28]

$$\Delta\gamma \propto B^2 \cdot \cos 2(\Phi_B - \Phi_2) \quad (1.3)$$

where B is magnetic field, Φ_B is the azimuthal angle of the magnetic field, Φ_2 is the second-order corresponding initial event-plane angles.

People used to think of there should be no charge separation caused by the CME effect in small systems collision due to the absence of azimuthal correlation between Φ_B and Φ_2 [29, 30]. In recent years experiment data show that the results of $\Delta\gamma$ in small system collision is very similar with heavy nuclear collision, such as Au+Au and Pb+Pb [19, 31], which implies that the main contribution of the charge anisotropy ($\Delta\gamma$) in $A + A$ collisions comes from the elliptical flow background (v_2) but not CME.

In order to clarify the contribution of CME, it is very necessary to study the nature of magnetic fields in small collision systems. The aim of this work is to give a more clear study on structure of event-by-event generated electromagnetic fields in small systems considering inner charge distribution of a nucleon. we focus on both the magnitude of the magnetic field \mathbf{B} and its azimuthal correlation $\langle \cos 2(\Phi_B - \Phi_2) \rangle$. Furthermore, we will show that $B^2 \cdot \cos 2(\Phi_B - \Phi_2)$ have a considerable value in small system.

We use the Lienard-Wiechert potentials to calculate the electric and magnetic fields:

$$\begin{aligned} e\mathbf{E}(\mathbf{t}, \mathbf{r}) &= \frac{e^2}{4\pi} \sum_n Z_n(\mathbf{R}) \frac{\mathbf{R}_n - R_n \mathbf{v}_n}{(R_n - \mathbf{R}_n \cdot \mathbf{v}_n)^3} (1 - v_n^2) \\ e\mathbf{B}(\mathbf{t}, \mathbf{r}) &= \frac{e^2}{4\pi} \sum_n Z_n(\mathbf{R}) \frac{\mathbf{v}_n \times \mathbf{R}_n}{(R_n - \mathbf{R}_n \cdot \mathbf{v}_n)^3} (1 - v_n^2) \end{aligned} \quad (1.4)$$

where $\mathbf{R}_n = \mathbf{r} - \mathbf{r}_n$ is the relative position of the field point \mathbf{r} to the source point \mathbf{r}_n , and \mathbf{r}_n is the location of the n th particle with velocity v_n at the retarded time $t_n = t - |\mathbf{r} - \mathbf{r}_n|$ [5]. The summations run over all charged particles in the system. Some theoretical uncertainties come from the modeling of the proton: treating the proton as a point charge or as a uniformly charged ball [32].

In paper [29], the authors have calculated the electromagnetic fields produced in small system, treating the nucleon as a point-like charge particle with a distance cut-off to avoid possible large fluctuation. In paper [30], the authors use a Gaussian function with $\sigma = 0.4$ fm to simulate the inner charge distribution of proton. Their results show that the magnetic field direction and the eccentricity orientation are uncorrelated. However, these models could eliminate huge fluctuation of fields strength effectively, but they are not good description of realistic inner charge density of nucleon and loss the possible correlation between Φ_B and Φ_2 . We will show that in this paper, while considering realistic charge density inside a nucleon, the electromagnetic fields produced by a flying single nucleon could be more complicated, and lead to an azimuthal correlation between Φ_B and Φ_2 in small collisions. In this work, we use three different charge density models to describe the proton and neutron, which are Point-Like model, Hard-Sphere model, and more physical Charge-Profile model.

This paper is organized as following: In section II we introduce three different charge density models of proton and neutron. In section III, we give the results of magnetic field produced by a single nucleon with RHIC energy observed in a lab reference. In section IV and section V, we began to calculate the magnetic field produced in high energy small collision p+A.

II. CHARGE DISTRIBUTION MODEL OF NUCLEON

In the calculation of electromagnetic field produced in high energy ion collisions, people used to treat nucleon as a Point-Like particle with a charge $+e$ for proton and 0 for neutron. This is the simplest simplification, and is a good approximation for heavy ion collisions. Because there are dozens of protons in these heavy ion collision system, the field produced by these nucleons are averaged among them, so the discrepancy from the charge profile of nucleon could be negligible.

However, this Point-Like model will bring a large numerical fluctuation to results in high energy ion collisions, especially for small collision system. In order to eliminate this numerical fluctuation, we introduce the second charge model for proton, Hard-Sphere model. In this model, the proton is treated as a sphere with homogeneous charge density.

$$\rho_p(r) = \begin{cases} \rho_0 & r \leq R \\ 0 & r > R \end{cases} \quad (2.1)$$

with $\rho_0 \approx 0.354 \text{ fm}^{-3}$, $R \approx 0.88 \text{ fm}$. While neutron is neutral, there should not be contribution to field from neutron within Point-Like model and Hard-Sphere model, so we didn't include neutrons into our calculation framework within these two models.

The Point-Like model and Hard-Sphere model are both simplifications for realistic inner charge distribution of proton. In order to discuss the field produced in small system more precisely, we need the physical 3-dimensional charge profile of nucleons, not only proton but also neutron, noted as Charge-Profile model.

Since the transverse charge density of proton and neutron are available in [33]:

$$\rho(b) = \int_0^\infty \frac{dQ}{2\pi} J_0(Qb) \frac{G_E(Q^2) + \tau G_M(Q^2)}{1 + \tau} \quad (2.2)$$

with $\tau = \frac{Q^2}{4M^2}$, M the mass of proton or neutron, J_0 a cylindrical Bessel function. Employing the parameterization of electric form factor G_E and magnetic form factor G_M [34] into Eq. (2.2), we can get the transverse charge density of proton and neutron shown in Fig. 1.

Based on the transverse charge density, we can get the 3-dimensional charge profile of proton and neutron after inverted convolution with a spherical symmetry approximation, shown in Fig. 2

III. MAGNETIC FIELD PRODUCED BY A SINGLE NUCLEON

With inner charge distribution models, we can investigate the space distribution of field produced by a single nucleon replacing the sum in Eq. (1.4) as integration. Given a single proton with 100 GeV which is corresponding to RHIC energy, traveling along $+z$ direction. With the 3-dimensional Charge-Profile

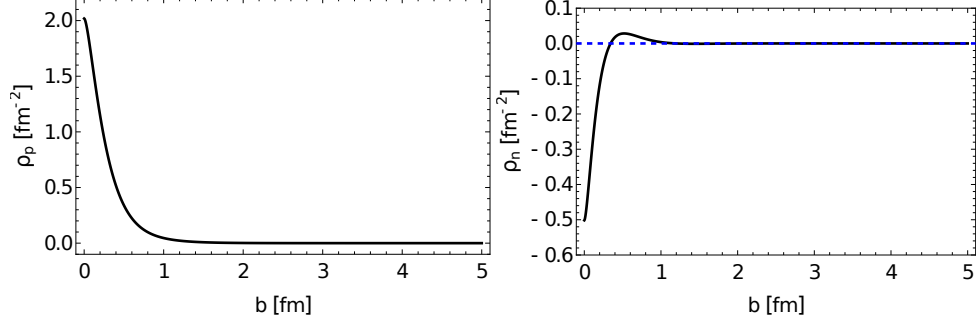


FIG. 1. The transverse charge density of proton (left) and neutron (right) in Charge-Profile model.

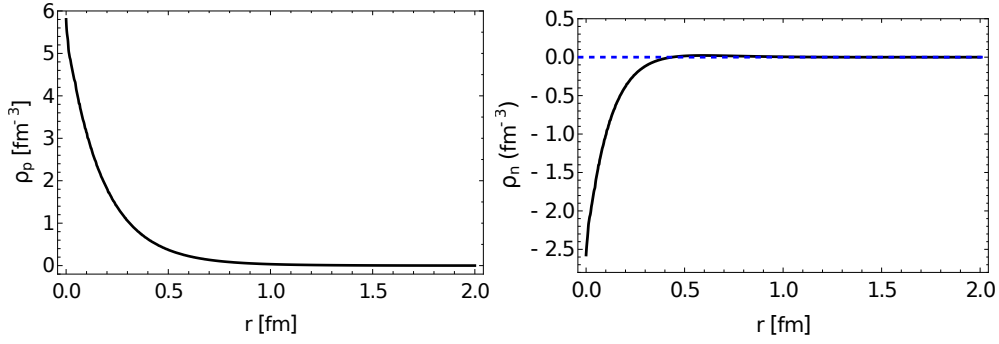


FIG. 2. The 3-dimensional charge profile of proton (left) and neutron (right) in Charge-Profile model.

model, the results are given in Fig. 3. Since this single proton travels with an ultra-relativistic speed, the space distribution of field is Lorentz contracted with a factor $\gamma = E/m$. So we show our results on $x - y$ plane with four different z locations.

In the first panel of Fig. 3, the $x - y$ distribution of B_y at $z = 0$ is shown. We can see the magnetic field at the central location $r = (0, 0, 0)$, just the center of this single proton, is not divergence but 0 exactly. While we increase the value of z , the strength of B_y is decreased. Shown on Fig. 3(d), we see the strength of B_y at $z = 10/\gamma$ fm is about three order smaller than that on $z = 0$.

Also, we checked the strength of B_y with Point-Like model. The corresponding results are shown on Fig. 4. In this calculation, we have abandoned the result at $r = (0, 0, 0)$ in order to eliminate divergence. We can find that the strength of B_y in Point-Like model is much larger than what in Charge-Profile model at small value of z , while the strength of B_y in the two models are similar at large z . From these calculation, we can see the results within Point-Like model could implement much larger fluctuation comparing with Charge-Profile model. For small collision system, because there are only a few nucleons have significant contribution to magnetic field, this fluctuation will bring us much trouble to handle on. And this fluctuation comes only from numerical calculation based on an unnecessary simplification. That's why it's necessary to introduce the physical Charge-Profile model to calculate electromagnetic field in this work.

In Point-Like model and Hard-Sphere model, neutron cannot contributed to electromagnetic field because of its neutral charge. But seeing from Fig. 2, neutron also has its charge profile. So neutron could also contribute to electromagnetic field in principle. Shown in Fig. 5, the space distribution of B_y is calculated within Charge-Profile model for neutron. the strength of field is finite and significant smaller than proton at

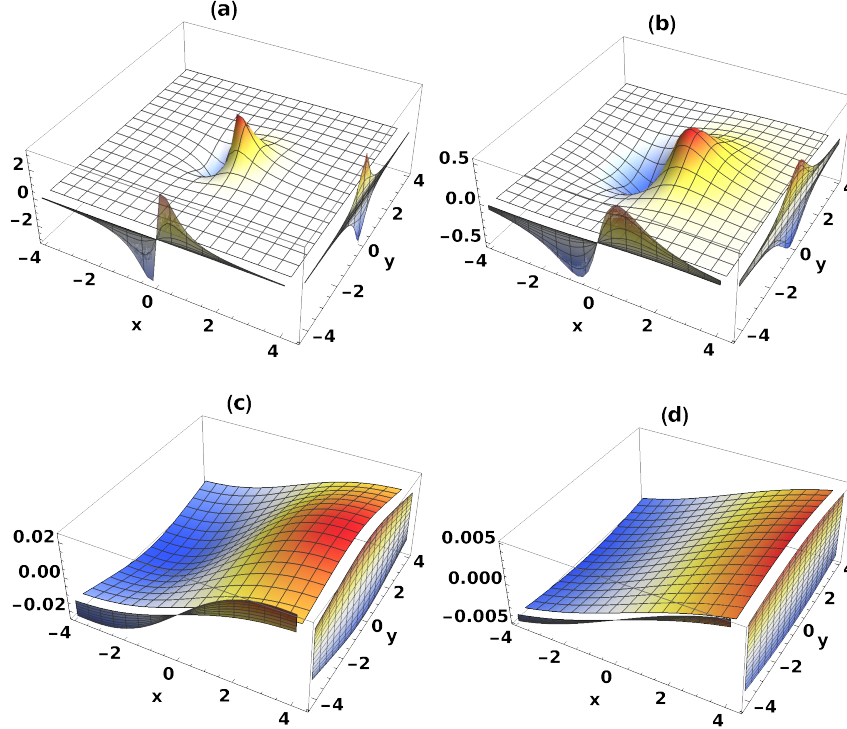


FIG. 3. The space distribution of magnetic field B_y on $x-y$ plane with $z = 0$ on Fig. 3(a), $z = 1/\gamma$ (fm) on Fig. 3(b), $z = 5/\gamma$ (fm) on Fig. 3(c), and $z = 10/\gamma$ (fm) on Fig. 3(d) produced by a single proton with 100 GeV travels through $+z$ direction, calculated within Charge-Profile model.

small z location, while it decrease rapidly to 0 at large z location. This is reasonable since neutron is charge neutral if it's measured from far away no matter what charge distribution in it.

IV. GEOMETRY CONFIGURATION OF SMALL COLLISION SYSTEM

From this section, we concentrate on the electric and magnetic field produced in high energy small collision system $p + A$. The collision geometry in our calculation is shown in Fig. 6, where b is the impact parameter which is the distance between the centers of two nuclear. In our framework, the single proton p is treated as projectile travels along $+z$ direction, while the heavy ion A is treated as target travels along $-z$ direction. we set z coordination pass through the center of b , and put the projectile at $x = b/2$ and target at $x = -b/2$.

Inside the heavy ion, the position of each nucleon is sampled according to Woods-Saxon distribution

$$\rho(r) = \frac{\rho_0}{1 + \exp[(r - R)/a]} \quad (4.1)$$

where $\rho_0 = 0.17 \text{ fm}^{-3}$, $a = 0.535 \text{ fm}$, R is the radius of coming heavy ion. Then the number of participants in each event could be determined from Monte-Carlo Glauber model.

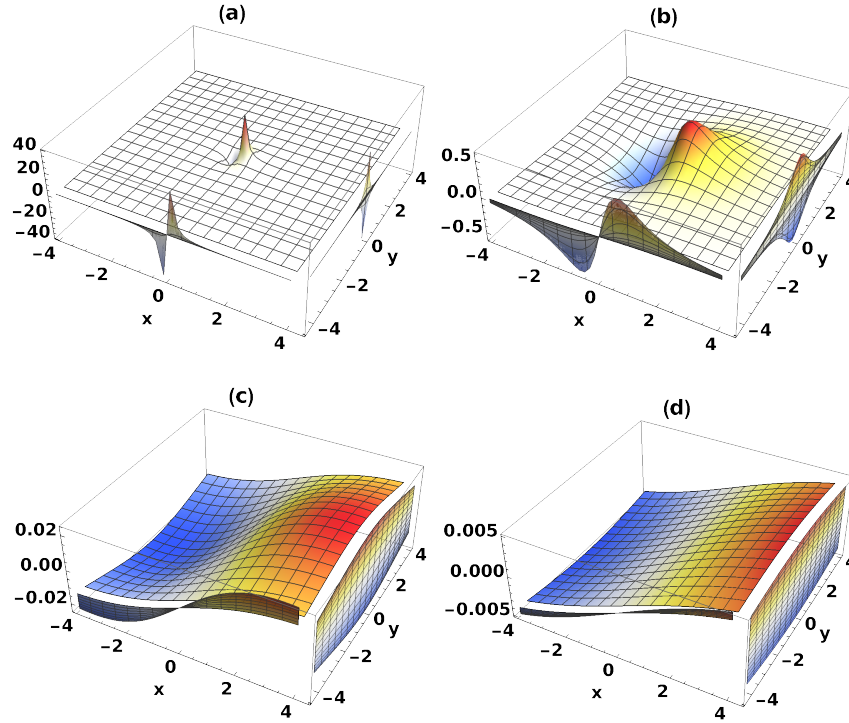


FIG. 4. The space distribution of magnetic field B_y on $x-y$ plane with $z = 0$ on Fig. 4(a), $z = 1/\gamma$ (fm) on Fig. 4(b), $z = 5/\gamma$ (fm) on Fig. 4(c), and $z = 10/\gamma$ (fm) on Fig. 4(d) produced by a single proton with 100 GeV travels through $+z$ direction, calculated within Point-Like model

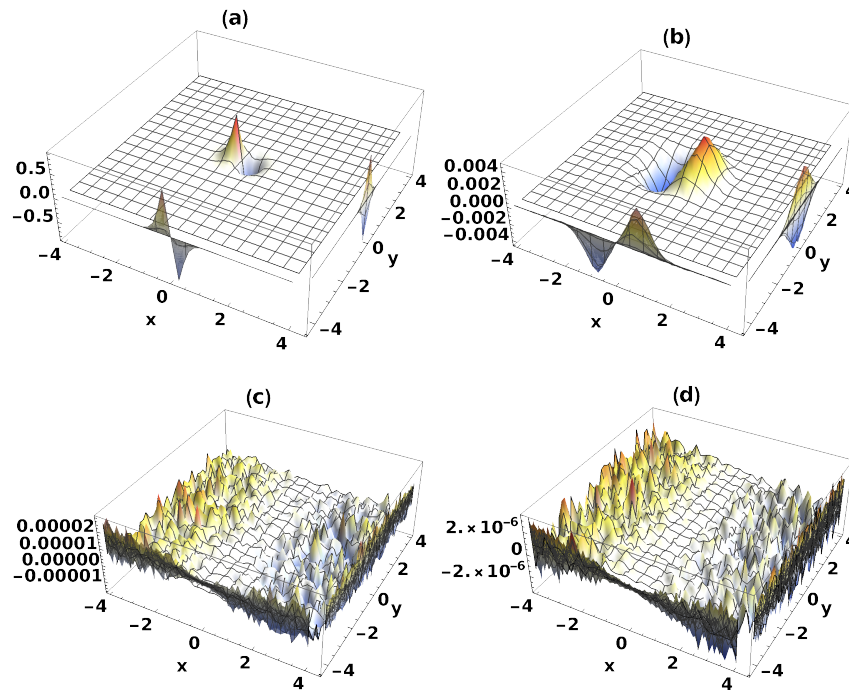


FIG. 5. The space distribution of magnetic field B_y on $x-y$ plane with $z = 0$ on Fig. 5(a), $z = 1/\gamma$ (fm) on Fig. 5(b), $z = 5/\gamma$ (fm) on Fig. 5(c), and $z = 10/\gamma$ (fm) on Fig. 5(d) produced by a single neutron with 100 GeV travels through $+z$ direction, calculated within Charge-Profile model.

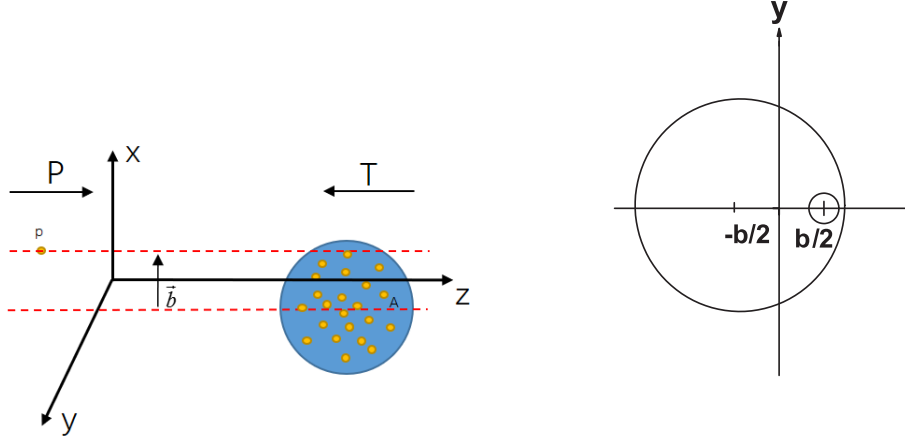


FIG. 6. The geometry of small collision system $p + A$.

V. RESULTS AND DISCUSSIONS

To understand and analyze theoretical uncertainties, we will calculate the $\langle E_x \rangle$, $\langle |B_x| \rangle$, $\langle -B_y \rangle$, and $\langle |B_y| \rangle$ using Point-Like model, Hard-Sphere model, and Charge-Profile model based on our available results of fields produced by single nucleon in section III. Here, the angle bracket is to denote event average. All results shown below are the strength of fields on location r_c which is the centre of mass of all participants.

A. Impact parameter dependence of fields

Firstly, in Fig. 7, we show the impact parameter dependence of the strength of fields produced within Point-Like model at RHIC energy. After averaged over 10^6 events, the value of E_x and B_y are shown (red curves in Fig. 7(a) and Fig. 7(b)) still with large fluctuation as we expected. After checking contributions from participants nucleons and spectators nucleons, we find that this large fluctuations come from participants.

In small collision system $p + A$, there are only a few participants in each event due to the small size of single projectile proton. So these participants are all near to the observation point r_c . The contribution from each participant to fields could has a large strength as shown in Fig. 4. But because the position of each nucleon is random inside nucleus, the orientation of this field contributed from each participant is almost azimuthal random. Then the total field summed over these participants could remain a large strength but azimuthal random. That's why there are so large fluctuations seen within Point-Like model.

In order to get the strength of fluctuation, we also calculate the impact parameter dependence of $|B_x|$ and $|B_y|$ shown on the Fig. 7(c) and Fig. 7(d). Seen from these two panels, the averaged fluctuations of fields are very large, which is almost 80 times larger than fields strength in Au+Au collisions at RHIC energy[5].

With Hard-Sphere model, the impact parameter dependence of fields are shown in Fig. 8. The curves in Fig. 8 are much smoother than what in Fig. 7. Seen from Fig. 8(c) and Fig. 8(d), the fluctuations are also

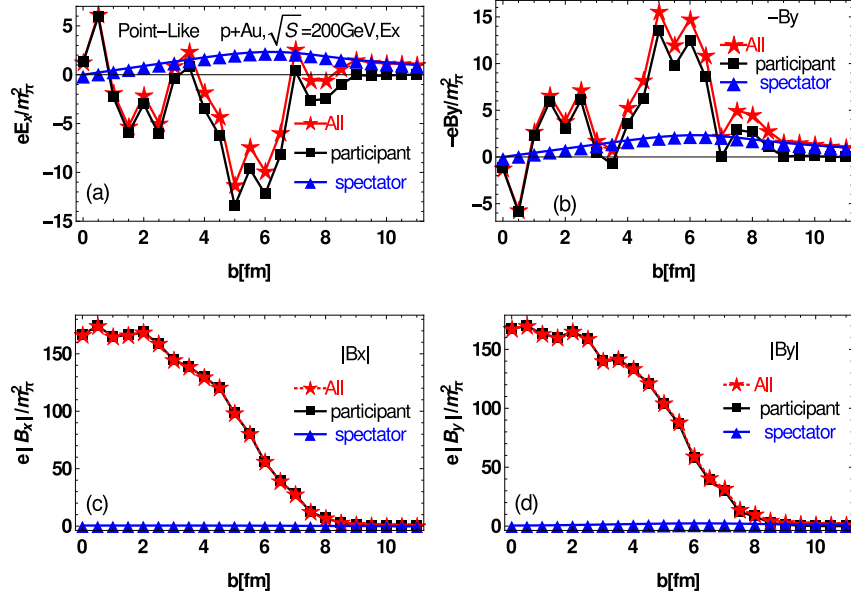


FIG. 7. The electromagnetic fields at $t=0$ and $\mathbf{r} = \mathbf{r}_c$ as function of the impact parameter b with Point-Like model.

much smaller than what in Point-Like model.

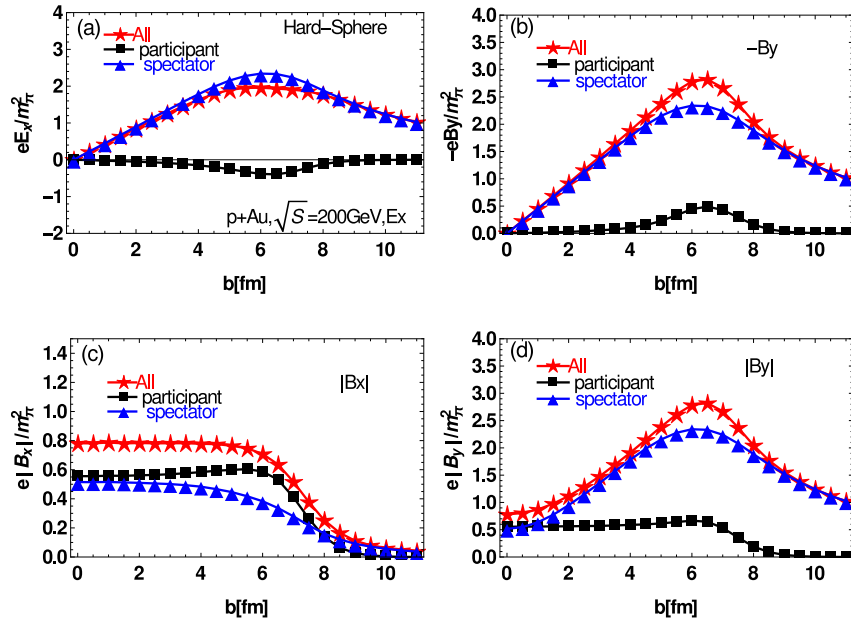


FIG. 8. The electromagnetic fields at $t=0$ and $\mathbf{r} = \mathbf{r}_c$ as function of the impact parameter b with Hard-Sphere model.

Shown on Fig. 8(b), total magnetic field B_y contributed mainly from spectators. The strength of total B_y and the strength from spectators are both increased with impact parameter, and have maximal values at $b \approx 6.5$ fm. While in Fig. 8(a), contribution from participants to E_x is negative in the range of impact parameter b between 2 and 8 fm. This is simply because that, the single projectile proton collisions on periphery of target nucleus in this range of b . So the center of mass \mathbf{r}_c is approximately geometry centre of

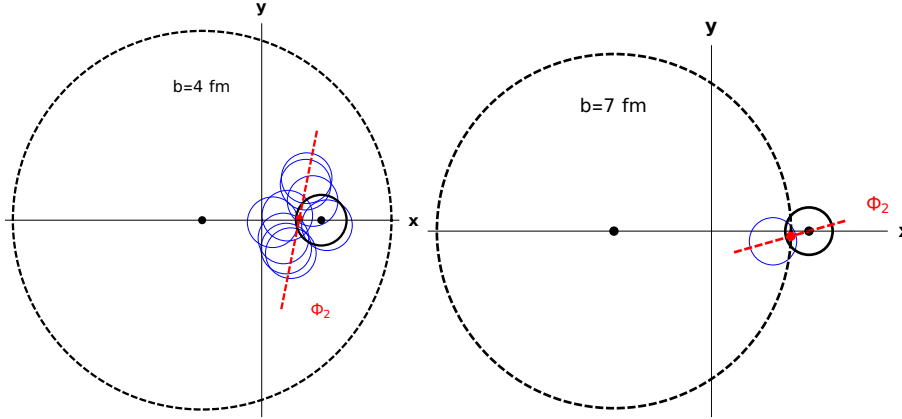


FIG. 9. Examples of participants distribution in one event with $b = 4$ fm (left panel), and $b = 7$ fm (right panel). The red point is centre of mass \mathbf{r}_c , and the red line indicates Φ_2 . The blue circles are participants from target nucleus, while the black circle is the single projectile proton.

all participants in each event, the single projectile proton prefer locating on $+x$ side of geometry centre, as shown in the illustration Fig. 9. After average over many events, contributions from target participants to E_x will offset with each other, but contribution from single projectile proton will remain along $-x$ direction.

In Fig. 10, results of impact parameter dependence of fields calculated with Charge-Profile model are given. Since the 3-dimensional charge density are given from electromagnetic form factors measured in experiments[34][33], these results are more physical than those with Hard-Sphere model.

Firstly, let's check the fluctuations with Charge-Profile model. Shown in Fig. 10(c) and Fig. 10(d), we can see fluctuation of fields from spectators are almost identical with that in Hard-Sphere model. That means the contribution from spectators are not sensitive to the detail of inner charge distribution of nucleon. This is because spectators are far away from \mathbf{r}_c , the discrepancy of inner charge density details can not be seen clearly. On the contrary, since all participants are near to \mathbf{r}_c , their contributions are not negligible, so the fluctuations from participants are quite different with that in Hard-Sphere model.

About the strength of electric fields E_x shown on Fig. 10(a), contribution from all participant is still negative, like that in Hard-Sphere model, since the contribution from single projectile proton remains along $-x$ direction. Its negative strength is so large that there is a significant depression to total E_x at $b \approx 6$ fm.

In Fig. 10(b), although strength of B_y contributed from spectators are still similar with Hard-Sphere model, the contribution from participants is quite larger. Especially in peripheral collisions, contributions from participants are even with same order with spectators. This is the main difference comparing with heavy ion $A + A$ collision system. Since the orientation of event plane is determined only by participants, this large contribution of participants to B_y maybe bring a significant azimuthal correlation between event plane Φ_2 and magnetic field Φ_B .

Comparing the magnetic strength of B_y in paper [30], our results within Charge-Profile model is about half. Considering the very small size of overlapping area in small collision system, any discrepancy in the inner charge density of nucleon could lead to a significant difference on fields strength. This could also be concluded while comparing Fig. 3(a) and Fig. 4(a). So, beyond the Hard-Sphere model, we also implement the realistic Charge-Profile model in our calculation.

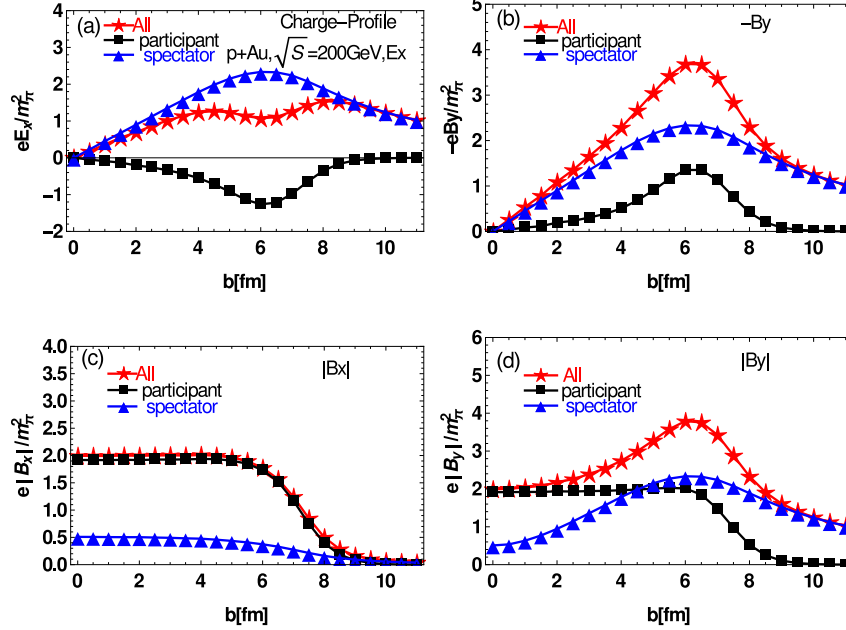


FIG. 10. The electromagnetic fields at $t=0$ and $\mathbf{r} = \mathbf{r}_c$ as function of the impact parameter b with Charge-Profile model.

B. Azimuthal correlation between \mathbf{B} and reaction plane

As we mentioned, $\Delta\gamma \propto B^2 \cdot \cos 2(\Phi_B - \Phi_2)$, where Φ_B is the angle of magnetic field \mathbf{B} direction. In this section we focus on the 2nd harmonic participant plane Φ_2 as it is the most prominent anisotropy from both geometry and fluctuations. The corresponding initial event plane angles are given by:

$$\Phi_n = \frac{1}{n} \arctan \frac{\langle r^n \sin(n\phi) \rangle}{\langle r^n \cos(n\phi) \rangle} \quad (5.1)$$

where r is the distance of the participants particles from the center of mass \mathbf{r}_c , ϕ is angle between the x direction and the direction of r [35]. We define Φ_2 as the long axis direction of the ellipse.

Our calculations in this subsection are all within Charge-Profile model to get a physical understanding of azimuthal correlation between Φ_B and Φ_2 . Firstly, we give the distribution of the discrepancy $\Phi_B - \Phi_2$ in Fig. 11. We can see there is a strong negative correlation between Φ_B and Φ_2 observed at large b , this is because there could be only one nucleon in target nucleus hit by single projectile proton in this very peripheral collision, as illustrated in right panel of Fig. 9. So the direction of Φ_2 (the long axis of ellipse) prefers near to x direction, which is perpendicular to the direction of magnetic field.

While at small and middle values of b , there is a slight but not negligible correlation between Φ_B and Φ_2 , even at $b = 0$ fm shown in the first panel on Fig. 11. This phenomenon could also be explained from left panel in Fig. 9. In each event, the contribution to fields from the single projectile proton is very large comparing to target participants since the centre of mass \mathbf{r}_c is very near to it. While the location of this single projectile proton prefers to $+x$ side of \mathbf{r}_c in event, its contribution to B_y prefers to $-y$ direction in each event. On the other hand, due to nuclear geometry, the target participants overlap as an approximate

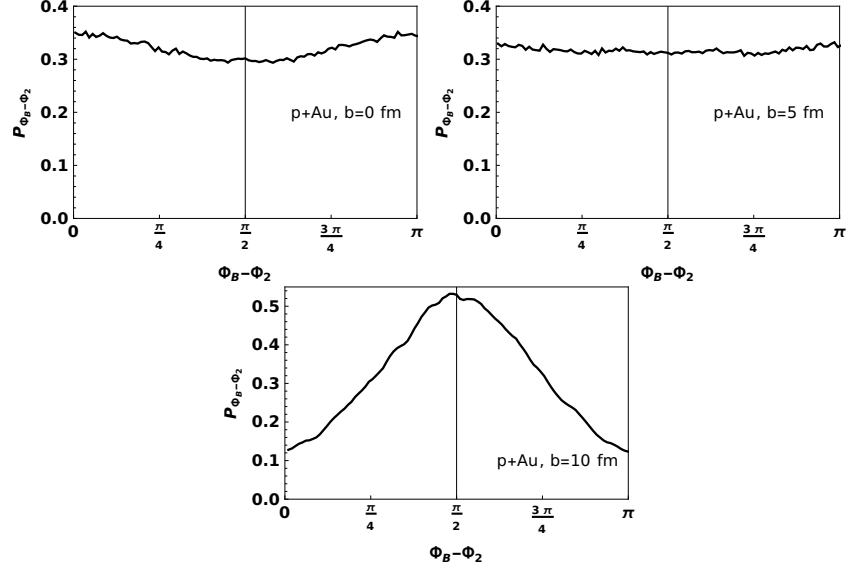


FIG. 11. The electromagnetic fields at $t=0$ and $r = r_c$ as function of the impact parameter b with Charge-Profile model.

ellipse with its long axis along y direction.

This correlation between Φ_B and Φ_2 could also shown in the azimuthal correlation factor $\cos 2(\Phi_B - \Phi_2)$, shown in left panel of Fig. 12. We can see the value of this correlation factor is very small but not vanished at small and middle range of impact parameter b . In large b range, the azimuthal correlation shown in the lower panel of Fig. 11 appears again here. This result is also consistent with paper[29].

Since the CME induced charge separation effect is described as $\Delta\gamma \propto B^2 \cdot \cos 2(\Phi_B - \Phi_2)$, We give this B^2 evolved azimuthal correlation in right panel of Fig. 12. Due to the large fluctuation of strength of

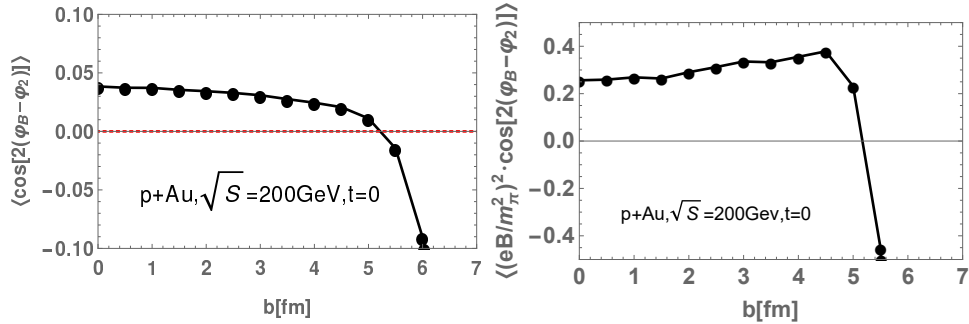


FIG. 12. The left panel is the azimuthal correlations between magnetic field plane Φ_B and Φ_2 , while the right panel is $B^2 \cdot \cos 2(\Phi_B - \Phi_n)$ as a function of impact parameter for $p + Au$ at RHIC energy .

magnetic field (Fig. 10(d)), the slight remaining azimuthal correlation could give a finite $\Delta\gamma$ signal due to the CME effect.

This calculation can be extended to LHC energy easily. We give corresponding results in Fig. 13. The result of azimuthal correlation $\cos 2(\Phi_B - \Phi_2)$ at LHC energy is similar with what at RHIC energy. While due to much more fluctuation of the strength of magnetic field, the B^2 evolved azimuthal correlation

$B^2 \cdot \cos 2(\Phi_B - \Phi_n)$ in LHC energy is three order larger than what in RHIC energy. With this strong

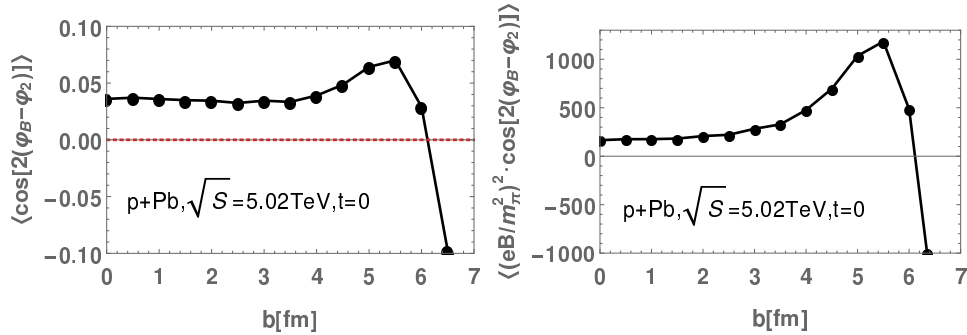


FIG. 13. The left panel is the azimuthal correlations between magnetic field plane Φ_B and Φ_2 , while the right panel is $B^2 \cdot \cos 2(\Phi_B - \Phi_n)$ as a function of impact parameter for $p + Pb$ in LHC energy .

azimuthal correlation between Φ_B and Φ_2 , it implies that the CME signals may be found in the small system, and maybe explain the observed $\Delta\gamma$ experiment data partly [19, 31].

VI. CONCLUSION

The contribution of CME to the charge separation effect related not only with the strength of magnetic field, but also with the angle between direction of magnetic field Φ_B and reaction plane Φ_2 . In the heavy ion small collision system with $p+A$ or $d+A$ collision, people used to believe that the direction of magnetic field is determined by the distribution of spectators mainly, while the direction of reaction plane is computed from the space distribution of participants. Due to the decoupling of angular correlation between the reaction plan and direction of magnetic field, this charge separation effect should be vanished. However, the experiment data show a quite different result comparing to theory predictions.

Employing a physical Charge-Profile model to describe the inner charge distribution of a proton and a neutron, we calculated the property of electromagnetic field produced in small system both in RHIC and LHC energy systematically, including its dependence on impact parameter b . Especially, we have studied the azimuthal correlation between Φ_B and Φ_2 carefully.

In conflict with people's previous expectations, our results show a significant angular correlation between them. This correlation comes mainly from the very close distance between the location of single projectile proton and the location of C.M.S r_c of hot medium produced in small collision system. Then the contribution of single projectile proton to the magnetic field is the main source after average over all participants. So the strong angular distribution priority of this single projectile proton could contribute significantly to the angular correlation of Φ_B and Φ_2 .

This discovery breakthrough people's previous thought about magnetic filed produced in small collision system. It can help us to clarify contribution of CME to the observation in small system collision experiments.

VII. ACKNOWLEDGMENTS:

We thank Xu-Guang Huang for very helpful discussions. We were supported by the NSFC under Projects No. 12075094 and No. 11535005.

-
- [1] J. Rafelski and B. Muller, *Phys. Rev. Lett.* **36**, 517 (1976).
 - [2] V. Skokov, A. Yu. Illarionov, and V. Toneev, *Int. J. Mod. Phys. A* **24**, 5925 (2009), arXiv:0907.1396 [nucl-th].
 - [3] A. Bzdak and V. Skokov, *Phys. Lett. B* **710**, 171 (2012), arXiv:1111.1949 [hep-ph].
 - [4] V. Voronyuk, V. D. Toneev, W. Cassing, E. L. Bratkovskaya, V. P. Konchakovski, and S. A. Voloshin, *Phys. Rev. C* **83**, 054911 (2011), arXiv:1103.4239 [nucl-th].
 - [5] W.-T. Deng and X.-G. Huang, *Phys. Rev. C* **85**, 044907 (2012), arXiv:1201.5108 [nucl-th].
 - [6] W.-T. Deng and X.-G. Huang, *Phys. Lett. B* **742**, 296 (2015), arXiv:1411.2733 [nucl-th].
 - [7] G. Inghirami, L. Del Zanna, A. Beraudo, M. H. Moggaddam, F. Becattini, and M. Bleicher, *Eur. Phys. J. C* **76**, 659 (2016), arXiv:1609.03042 [hep-ph].
 - [8] L. Yan and X.-G. Huang, (2021), arXiv:2104.00831 [nucl-th].
 - [9] D. Kharzeev, R. D. Pisarski, and M. H. G. Tytgat, *Phys. Rev. Lett.* **81**, 512 (1998), arXiv:hep-ph/9804221 [hep-ph].
 - [10] D. Kharzeev, *Phys. Lett. B* **633**, 260 (2006), arXiv:hep-ph/0406125 [hep-ph].
 - [11] D. E. Kharzeev, L. D. McLerran, and H. J. Warringa, *Nucl. Phys. A* **803**, 227 (2008), arXiv:0711.0950 [hep-ph].
 - [12] K. Fukushima, D. E. Kharzeev, and H. J. Warringa, *Phys. Rev. D* **78**, 074033 (2008), arXiv:0808.3382 [hep-ph].
 - [13] D. E. Kharzeev, J. Liao, S. A. Voloshin, and G. Wang, *Prog. Part. Nucl. Phys.* **88**, 1 (2016), arXiv:1511.04050 [hep-ph].
 - [14] Y.-C. Liu and X.-G. Huang, *Nucl. Sci. Tech.* **31**, 56 (2020), arXiv:2003.12482 [nucl-th].
 - [15] S. A. Voloshin, *Phys. Rev. C* **70**, 057901 (2004), arXiv:hep-ph/0406311 [hep-ph].
 - [16] B. I. Abelev *et al.* (STAR), *Phys. Rev. Lett.* **103**, 251601 (2009), arXiv:0909.1739 [nucl-ex].
 - [17] B. I. Abelev *et al.* (STAR), *Phys. Rev. C* **81**, 054908 (2010), arXiv:0909.1717 [nucl-ex].
 - [18] L. Adamczyk *et al.* (STAR), *Phys. Rev. Lett.* **113**, 052302 (2014), arXiv:1404.1433 [nucl-ex].
 - [19] A. M. Sirunyan *et al.* (CMS), *Phys. Rev. C* **97**, 044912 (2018), arXiv:1708.01602 [nucl-ex].
 - [20] S. Acharya *et al.* (ALICE), *Phys. Lett. B* **777**, 151 (2018), arXiv:1709.04723 [nucl-ex].
 - [21] H.-J. Xu, X. Wang, H. Li, J. Zhao, Z.-W. Lin, C. Shen, and F. Wang, *Phys. Rev. Lett.* **121**, 022301 (2018), arXiv:1710.03086 [nucl-th].
 - [22] L. Adamczyk *et al.* (STAR), *Phys. Rev. C* **89**, 044908 (2014), arXiv:1303.0901 [nucl-ex].
 - [23] F. Wang and J. Zhao, *Phys. Rev. C* **95**, 051901 (2017), arXiv:1608.06610 [nucl-th].
 - [24] N. N. Ajitanand, R. A. Lacey, A. Taranenko, and J. M. Alexander, *Phys. Rev. C* **83**, 011901 (2011), arXiv:1009.5624 [nucl-ex].
 - [25] A. Bzdak, *Phys. Rev. C* **85**, 044919 (2012), arXiv:1112.4066 [nucl-th].
 - [26] J. Zhao, H. Li, and F. Wang, (2017), arXiv:1705.05410 [nucl-ex].
 - [27] J. Błoczyński, X.-G. Huang, X. Zhang, and J. Liao, *Phys. Lett. B* **718**, 1529 (2013), arXiv:1209.6594 [nucl-th].
 - [28] J. Błoczyński, X.-G. Huang, X. Zhang, and J. Liao, *Nucl. Phys. A* **939**, 85 (2015), arXiv:1311.5451 [nucl-th].
 - [29] X.-L. Zhao, Y.-G. Ma, and G.-L. Ma, *Physical Review C* **97**, 10.1103/physrevc.97.024910 (2018).
 - [30] R. Belmont and J. L. Nagle, *Phys. Rev. C* **96**, 024901 (2017), arXiv:1610.07964 [nucl-th].
 - [31] V. Khachatryan *et al.* (CMS), *Phys. Rev. Lett.* **118**, 122301 (2017), arXiv:1610.00263 [nucl-ex].
 - [32] W.-T. Deng, X.-G. Huang, G.-L. Ma, and G. Wang, *Phys. Rev. C* **94**, 041901 (2016), arXiv:1607.04697 [nucl-th].
 - [33] G. A. Miller, *Ann. Rev. Nucl. Part. Sci.* **60**, 1 (2010), arXiv:1002.0355 [nucl-th].

- [34] W. M. Alberico, S. M. Bilenyk, C. Giunti, and K. M. Graczyk, *Phys. Rev.* **C79**, 065204 (2009), [arXiv:0812.3539 \[hep-ph\]](#).
- [35] W.-T. Deng, Z. Xu, and C. Greiner, *Phys. Lett.* **B711**, 301 (2012), [arXiv:1112.0470 \[hep-ph\]](#).